Journal of Petroleum Science and Technology 15(1): 45, 2025, Pages 72-79
DOI:10.22078/jpst.2025.5817.1993

Journal of Petroleum Science and Technology
Research Paper
https://jpst.ripi.ir/

Tracking the Dispersed Phase in Solid–Liquid Two-Phase Flow Using Digital X-Ray Imaging and the CSRT Tracking Algorithm in Python

Mohsen Sharifzadeh*, Mojtaba Askari, Amir Mohammad Beigzadeh, and Hadi Ardini
Radiation Application Research School, Nuclear Science and Technology Research Institute, Tehran, Iran

Abstract
The dispersed-phase velocity measurement module in two-phase flow is one of the most critical components of a two-phase flowmeter, particularly for monitoring oil, gas, and pipeline-transported products. Moreover, compared with conventional velocimetry methods, digital X-ray imaging offers a novel solution due to its ability to penetrate opaque materials, its high sensitivity to density variations, and its ability to rapidly image dynamic processes. By employing advanced image-processing algorithms, the dispersed phase can be effectively identified and tracked. This study investigates the feasibility of tracking and computing the trajectory equation of the dispersed phase by integrating digital X-ray imaging with the CSRT (Discriminative Correlation Filter with Channel and Spatial Reliability) tracking algorithm. The innovation of this research lies in applying image-processing algorithms to compute particle trajectories in multiphase flow metering systems. When the proposed method was implemented in Python, the method achieved particle detection and tracking accuracy of 94.7% with an error below 3%, under laboratory conditions. Ultimately, the results demonstrate that combining digital X-ray imaging with the CSRT tracking algorithm enables trajectory recognition of dispersed particles with a maximum error of ±5%.

Keywords: Tracking, Dispersed Phase, Two-Phase Flow, Digital Imaging, X-Ray, CSRT Algorithm, Python.

Introduction
Two-phase flows containing a dispersed dense phase are common in many industries, including nuclear, oil and gas, and food processing. Moreover, these flows are characterized by the presence of solid particles or liquid droplets suspended in a continuous carrier fluid (gas or liquid). In addition, the dynamic interactions between the dispersed and continuous phases significantly affect momentum, heat, and mass transfer, making their study essential for optimizing engineering systems. As shown in Equation 1, digital X-ray imaging is an effective method for determining the trajectory equation of representative particles in two-phase flow. This advantage arises from the exponential dependence of relative attenuation, I/I_0, on the product of the linear attenuation coefficient, μ, and the path length, x. In contrast to visible light, which cannot penetrate thick steel pipelines, X-ray imaging offers a superior option for analyzing particle trajectories within industrial flow systems [1, 2]:

$$I=I_0 e^{-\mu.x} \quad (1)$$

Digital X-ray radiography has emerged as a pivotal tool across diverse scientific fields, offering non-destructive imaging capabilities for structures, compositions, and processes. Fig. 1 illustrates the X-ray tube, the object, and the flat-panel detector positioned opposite the X-ray generator, arranged to perform the imaging process.
Recently, numerous studies have investigated the use of X-ray radiography to measure two-phase flow. Furthermore, these approaches primarily focus on extracting information about the spatial and temporal distribution of flow components and on tracking the dispersed phase. Moreover, Lasheras et al., Marmottant and Villermaux, Varga et al., and Schumaker et al. examined the imaging of asymmetrically injected sprays within pipe cross sections. Also, their findings indicated that variations in the relative gas to liquid phase fraction did not significantly affect the spray width [3–6]. In addition, the distinction between floating and slug flow regimes has recently been examined using three-dimensional X-ray imaging with a fan-beam collimated source and three fixed detectors [7]. Furthermore, Escudero and Heindel investigated the influence of acoustic oscillations on the particle volume fraction in a fluidized bed using three-dimensional X-ray imaging. Their results showed that acoustic vibration led to a more uniform particle volume fraction [8].

**Corresponding author:* Mohsen Sharifzadeh, *Radiation Application Research School, Nuclear Science and Technology Research Institute, Tehran, Iran*
E-mail addresses: mssharifzadeh@aeoi.org.ir
Received 2025-12-21, Received in revised form 2025-12-21, Accepted 2025-12-21, Available online .....

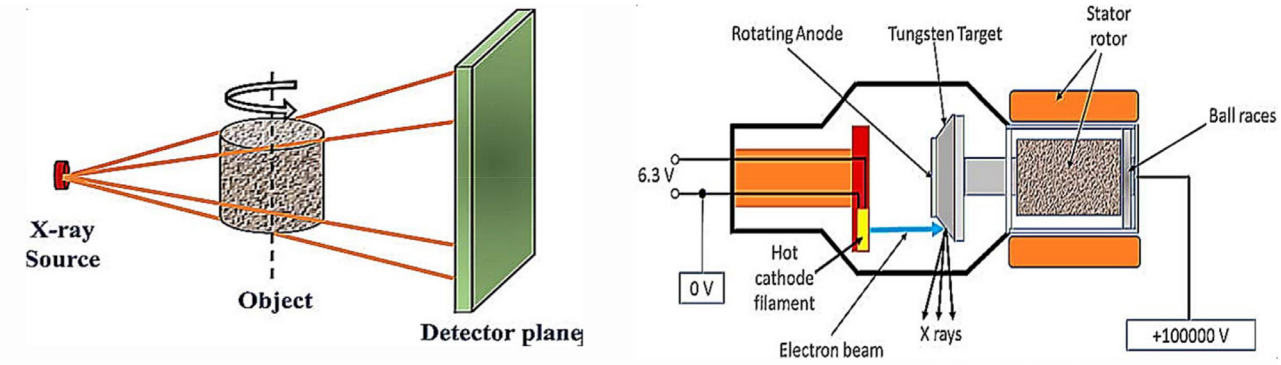

Fig. 1 View of an X-ray tube (right) and the imaging setup in digital radiography (left).

In a study by Alanazi et al. the optimal X-ray tube voltage was determined to enhance the accuracy and efficiency of intelligent two-phase flow imaging systems [9]. In a comprehensive 2021 review, Aliseda et al. highlighted the most commonly investigated multiphase flows—such as sprays, fluidized beds, and bubble columns—and emphasized advances in X-ray imaging for understanding the internal structure and multiphase interactions of these flows. Furthermore, they also discussed the potential of advanced tomography, time-resolved imaging, and particle tracking for future multiphase flow studies [10].

In a Monte Carlo simulation, Salgado et al. employed an artificial neural network to determine the volume fractions of oil–water–gas three-phase flow components using a single X-ray tube and two flat-panel detectors to count transmitted and scattered photons [11]. Fiore et al. described a novel radiation source based on X-ray fluorescence and used its emission energy spectrum to measure flow rates under challenging wet-gas conditions [12].

Misawa et al. in 2022 introduced the concept of high-speed X-ray tomography, its hardware development, and results from gas–liquid two–phase flow measurements in a vertical pipe. Moreover, their system used 18 pulsed X-ray sources, sequentially activated, producing a complete set of 18 independent images of the target object within 38 milliseconds [13]. In addition, Mingming et al. (2022) investigated the use of short, high-flux synchrotron pulses for dynamic imaging of multiphase flows, enabling density and velocity measurements via X-ray diffraction, followed by advanced image processing [14].

Finally, Roshani et al. (2021) evaluated the feasibility of using X-ray tubes instead of radioisotopic sources to measure the volume fractions of gas, oil, and water in two common three-phase flow regimes: annular and stratified. Moreover, the proposed detection system consisted of an X-ray tube, a sodium iodide detector, and a Pyrex glass pipe to simulate different volume fractions under the specified flow regimes. Furthermore, a group data processing method, considered a powerful regression tool, was applied to analyze the acquired data [15].

Tracking tracer particles across short sequences of time frames is recognized as an open and challenging problem in the field of computer vision, where Discriminative Correlation Filters (DCF) have demonstrated strong performance. In the study by Lukezic et al., the concepts of channel reliability and spatial reliability were introduced into DCF-based tracking, along with an innovative learning algorithm to efficiently and uniformly integrate them into the filter update and tracking process. The spatial reliability map aligns the filter's support region with the portion of the object most suitable for tracking, thereby enabling the tracking of non-rectangular objects and expanding the search region [16].

The distinctive contributions and innovations of the present research lie in integrating image-processing algorithms with digital X-ray imaging to determine the trajectory equation of tracer particles serving as the carrier phase in two-phase flow. The use of tracking algorithms developed through the intelligent fusion of color-channel information and spatial reliability represents a novel approach to object tracking in video frames. In this investigation, a setup consisting of an X-ray generator, a solid–liquid two–phase analog, and a flat panel detector was employed to acquire sequential images of solid tracer particles moving along different trajectories. Subsequently, an appropriate tracking algorithm was applied to determine the particle trajectories. Finally, by comparing the computed trajectory equations with the actual trajectories, the measurement accuracy of the proposed system in tracer particle tracking was reported.

Materials and Methods

X-ray Tube

In this study, an industrial X-ray generator model MXR 301 was employed, operating at 100 kV tube voltage and 1 mA tube current. Moreover, the tube can operate at a maximum voltage of 300 kV, a maximum current of 5 mA, and a focal spot size of 1 mm. Fig. 2 illustrates the X-ray generator along with its analog control interface. In addition, the maximum operating voltage of 300 kV enables penetration through thick materials, while the maximum current of 5 mA provides sufficient radiation for producing high-quality images. The device's output power is typically around 1.5 kW, suitable for precise and versatile imaging applications. Also, the generator's duty cycle is approximately 50%, allowing intermittent operation without overheating.

Tube Calibration

0Subsequently, the effect of voltage variations on image resolution and contrast was evaluated using the Balleau phantom illustrated in Fig. 3. Moreover, the detector exhibits a spatial resolution of 140 µm, and, using the phantom shown below, the finest line patterns corresponding to index 800 (highlighted by the yellow arrow) were clearly discernible. The line dimensions at indices 100 and 800 for this phantom are provided in Table 1.

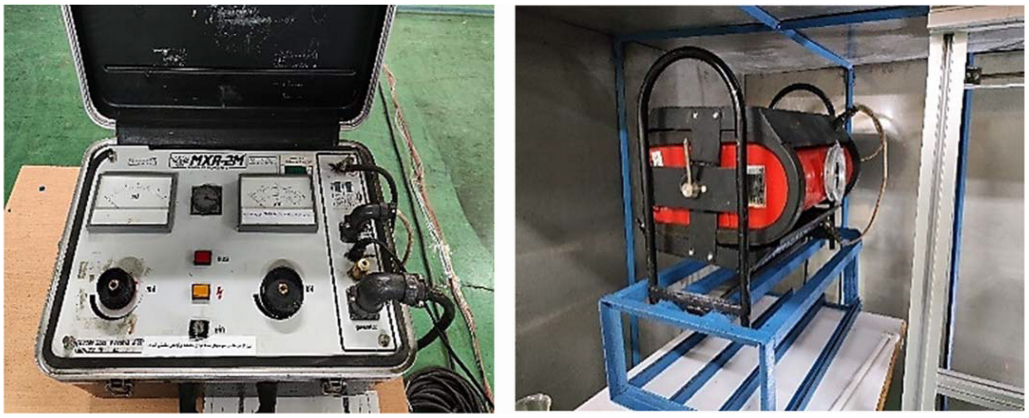

Fig. 2 View of the X ray generator (right) and its analog control interface (left).

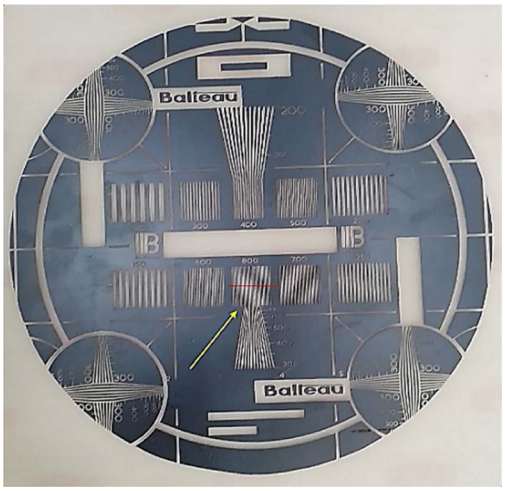

Fig. 3 Phantom employed for tube calibration.

Table 1 Line width dimensions at indices 100 and 800 of the resolution phantom.

Line strip number	Line width (μm)
100	2300
800	287.5

Flat-panel Detector

In Fig. 4, the Illustration of the Whale4343FOI flat-panel detector is seen. In addition, this figure shows the detector's capability for fine detail recognition in imaging.

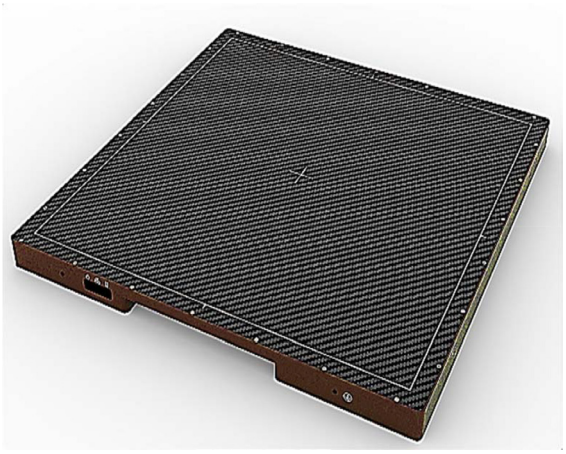

Fig. 4 View of the Whale 4343 FOI flat-panel detector.

With an active area of 430 × 430 mm, the detector enables precise detail recognition in images through its 140 μm pixel size. In addition, its imaging speed of up to 24 frames per second makes it a suitable option for real-time imaging. Also, the technical specifications of this detector are presented in Table 2.

Image Processing Software

In this study, the "XDiscoveryPro" software was used to manage and process images acquired by the detector. This software, developed by HAOBO Imaging Technology, serves as the primary platform for processing images obtained from flat-panel detectors with high frame rates of up to 20 frames per second. For communication with the detector, the software utilizes optical fiber interfaces, enabling high-speed data transfer and reducing noise. Furthermore, automatic offset and gain correction within the software compensates for minor image defects, thereby enhancing clarity and reducing noise.

The raw data from each frame were collected in "RAW" file format, stored as continuous frames, and subsequently transferred to MATLAB for further processing. Moreover, the numerical values in these files, representing photon flux per image pixel, were stored as a matrix using the "fread" function, which reads raw binary data.

In this research, a median filter was applied to suppress isolated single-pixel and discontinuous noise while preserving image edges. Moreover, a Gaussian filter was employed to reduce overall noise, smooth the image, and eliminate low-frequency noise. In addition, to improve image contrast and better visualize density variations in the phantom sample, histogram equalization was used. Furthermore, this technique redistributes pixel intensities, thereby enhancing contrast and revealing finer image details. Finally, the Canny edge detection algorithm was implemented to identify boundaries between regions with different densities.

Measurement Table

A measurement table was implemented to hold the X-ray generator, detector, and sample in alignment. In addition, the table includes a rotary stage, a motor for rotation, and bearings to ensure precise positioning and smooth motion. An illustration of this table is presented in Fig. 5.

Table 2 Technical specifications of the Whale4343FOI flat-panel detector.

Technology		Technical performance	
Sensor	Amorphous silicon	Resolution	3.5-line pairs per millimeter (lp/mm)
Scintillator	Gadolinium oxysulfide / Cesium iodide	Energy range	kV 160–40
Active Area	mm 430 × 430	Mechanical properties	
Pixel Pitch	µm 140	Dimensions	mm 5/32 × 470 × 470
User Interface		Weight	kg 9.5
Data Transfer	Optical fiber	Power	
Frame Rate	24 frames per second (fps)	Power supply	V AC 240–100
User-Environment	Windows 7/Windows 10 32/64-bit	Frequency	Hz 50/60

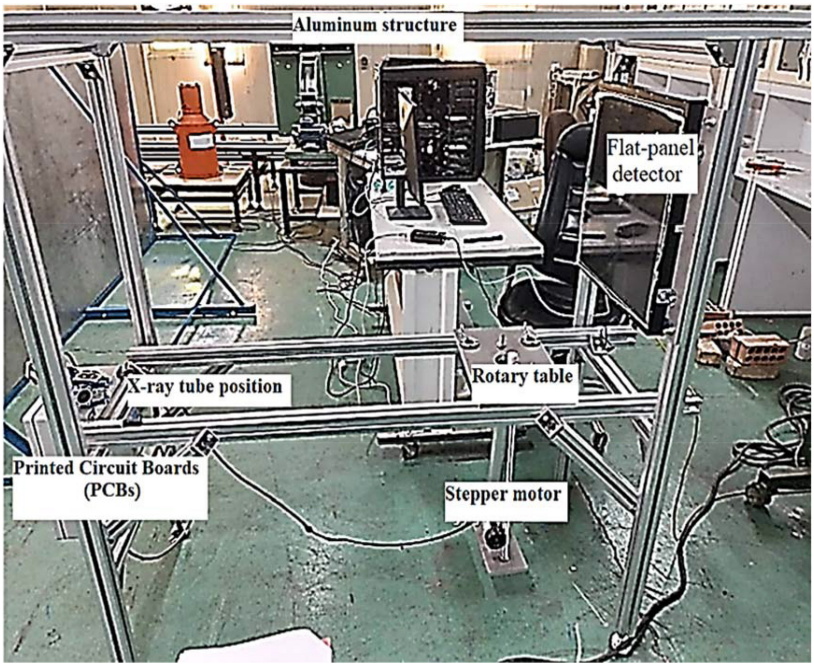

Fig. 5 View of the measurement table.

The structure was designed to ensure that all components interact coherently, enhancing the quality and accuracy of the acquired images. Moreover, the X-ray generator is positioned on one side of the structure, directing radiation toward the object or sample under investigation. Furthermore, the flat-panel detector is mounted on the opposite side of the structure, directly aligned with the X-ray beam. Also, at the center of the structure, a rotary table is placed to hold the sample. In addition, this table can rotate, allowing the system to acquire images from multiple angles. Moreover, a shielding enclosure surrounds the system, serving as a protective barrier to ensure operator safety and to prevent unnecessary radiation exposure to surrounding areas. The dimensional specifications of this table are provided in Table 3.

Table 3 Dimensional specifications of the measurement table.

Dimensional specifications of the measurement table	Dimensions
Distance from the X-ray generator to the phantom sample (cm)	124
Distance from the phantom sample to the array detector (cm)	36
X-ray beam irradiation angle (°)	0-90
Dimensions of the radiation shielding enclosure (m^2)	3×1.5
Thickness of the steel enclosure walls (mm)	4

Equivalent Solid–liquid Two-phase Flow

To simulate the motion of solid tracer particles in a solid–liquid two-phase flow, three plastic tubes were mounted on a flat polystyrene plate. Fig. 6 shows the three pathways along with their installation and positioning in front of the detector. Moreover, after all tubes were filled with water, three metallic beads were released at the top of each tube. Furthermore, these beads moved along three distinct paths with predetermined and fixed trajectories, passing through the X-ray beam field. In addition, the detector acquired its two-dimensional digital images, which were subsequently used for particle tracking via an image-processing algorithm. The selection of these solid tracer particles was made to overcome limitations caused by the absence of a test loop in the laboratory. Moreover, the objective of this study was to investigate the feasibility of tracking tracer particles using the proposed integrated system. In addition, the actual trajectories of the three pathways were obtained by successive, close-point sampling of the acquired digital images. Furthermore, 1 mm-diameter metallic beads, initially fixed at the top of each path using pins, were released into the transparent, water-filled plastic tubes after the generator and detector were prepared. Their motion then commenced, and by sequentially imaging the bead's movement along the three paths, the tracking algorithm extracted the trajectory equations.

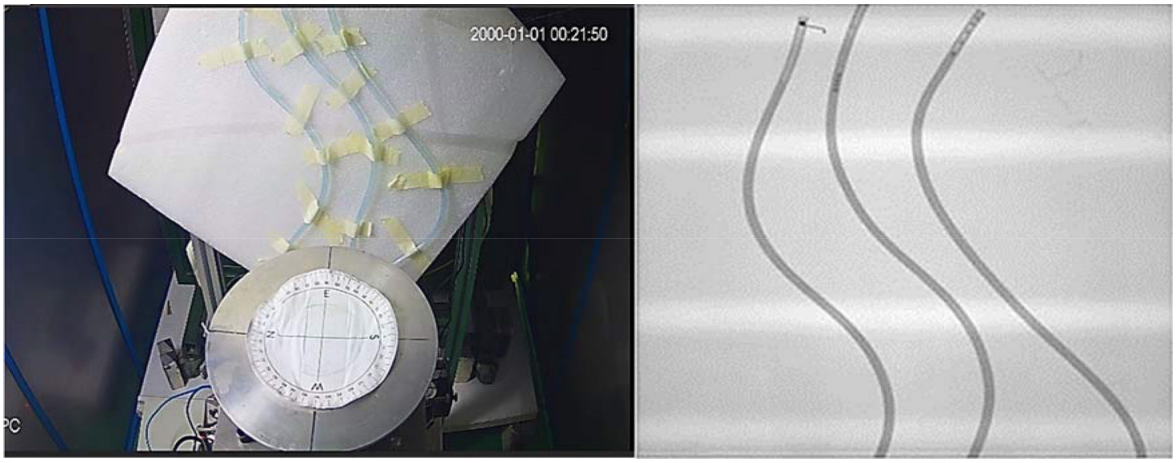

Fig. 6 View of the three pathways: plastic tubes mounted on a flat polystyrene background (left), and their digital image (right).

CSRT Tracking Algorithm

The CSRT tracking algorithm is a novel approach to object tracking across video frames. Moreover, it has been developed through the intelligent integration of color channel information and spatial reliability. In addition, by extracting multiple features from different channels (including color and gradient) and applying reliability weights to each channel, CSRT demonstrates high robustness to common challenges such as illumination changes, partial occlusions, and complex backgrounds.

Moreover, by identifying reliable regions within the object's search area, CSRT increasingly focuses on the target's more stable parts, leading to a significant improvement in tracking accuracy compared to conventional methods. At its core, CSRT employs a Discriminative Correlation Filter (DCF), an efficient learning algorithm that seamlessly integrates spatial and channel features into the filter update and tracking process. This filter constructs a comprehensive probabilistic model of the target object, enabling detection and adaptation to changes in its shape and size.

Another noteworthy aspect of CSRT's design is the use of a dual update mechanism. In this mechanism, one of the model's parts is continuously updated to adapt to appearance variations of the object, while another part maintains long-term stability to prevent gradual tracking drift. This delicate balance between adaptability and stability makes CSRT an effective and reliable choice for practical applications in dynamic and unpredictable environments.

Results and Discussion

X-ray Generator Calibration

Subsequently, Fig. 7 shows the recorded images of the phantom in Fig. 3 at a tube current of 1 mA and tube voltages of 80, 120, and 160 kV.

As shown in the figure above, increasing the tube voltage improves image clarity and makes the phantom details more distinguishable. Subsequently, the intensity variations resulting from voltage changes were plotted for the red line shown in Fig. 8 and compared.

The plot above shows that the recorded intensity in the detector pixels increased by a factor of 5.6 as the tube voltage increased from 80 to 160 kV. Based on these results, a tube current of 1 mA and a tube voltage of 160 kV were subsequently employed for imaging.

Real-time Images of the Beads

Fig. 9 shows the sequential images of the motion of metallic beads within the three helical paths. These images were acquired at three successive time points, and by employing the algorithm's locking mechanism on each bead, the trajectories of the beads were tracked.

Fig. 7 Recorded images of the X-ray generator calibration phantom at a tube current of 1 mA and tube voltages of 80 kV (top-left), 120 kV (top-right), and 160 kV (bottom).

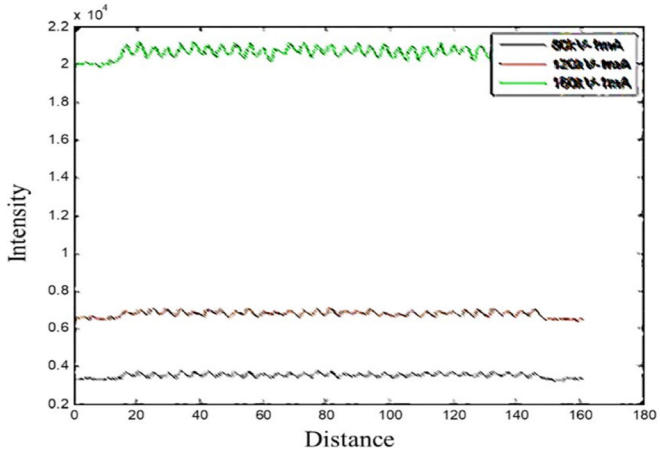

Fig. 8 Plot of the recorded intensity variations across the width of the red line corresponding to index 800 of the X-ray generator calibration phantom, as a function of tube voltage.

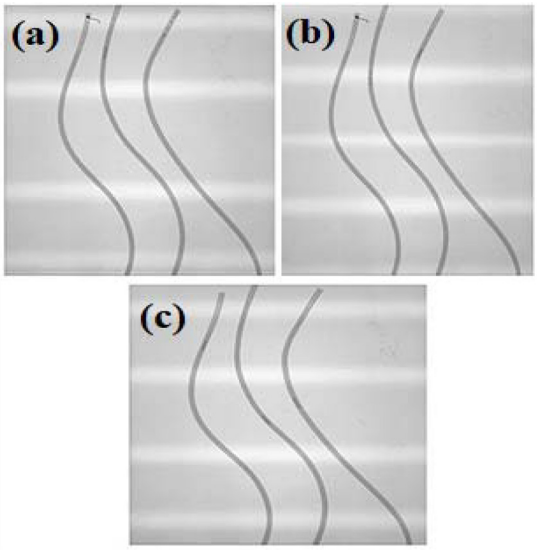

Fig. 9 Sequential images recorded from the motion of metallic beads within the three helical paths at time intervals t1 (a), t_2 (b), and t_3 (c), with the temporal condition $t1 < t_2 < t_3$.

Subsequently, after acquiring images of the bead motion, the bead's spatial position in successive time frames was calculated using the tracking algorithm. Furthermore, by sampling closely spaced points along each of the three paths, the actual trajectory equations were determined for comparison with the values extracted from image processing and algorithm application. Fig.s 10, 11, and 12 illustrate the actual and tracked trajectories of the beads along the left, middle, and right paths, respectively, used to compute both the real trajectory equations and the diagnostic trajectories obtained by the tracking algorithm.

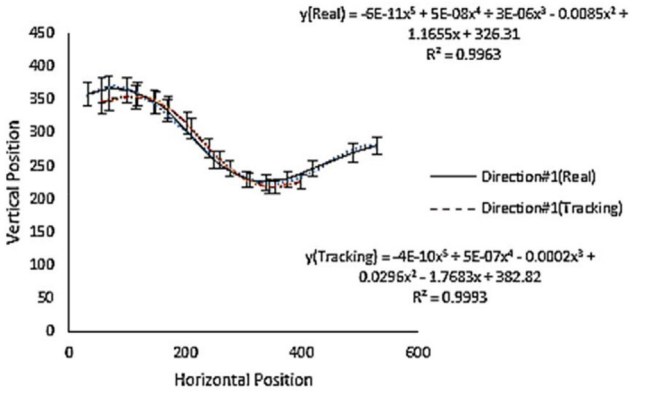

Fig. 10 Actual and tracked trajectories of the bead in the left path, as shown in the images of Fig. 9.

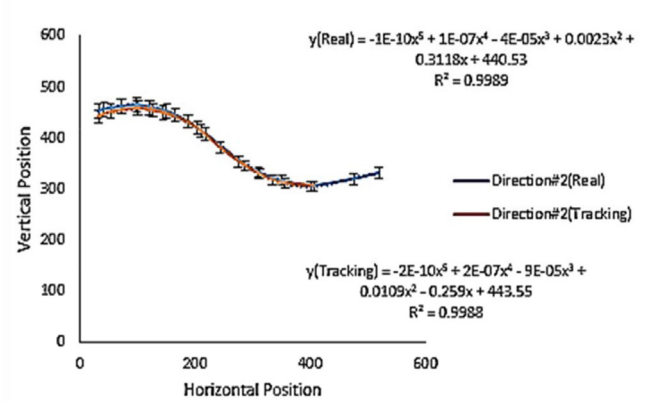

Fig. 11 Actual and tracked trajectories of the bead in the middle path, as shown in the images of Fig. 9.

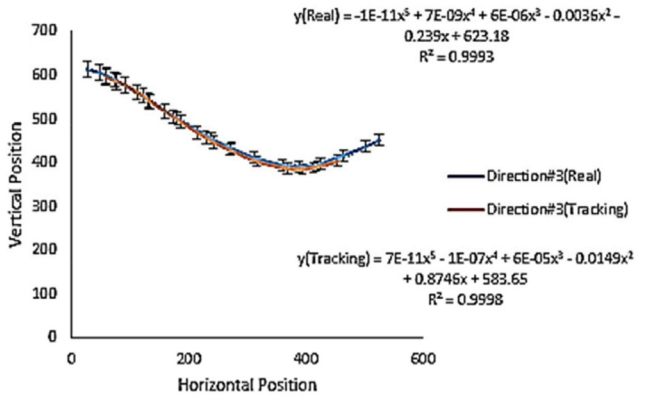

Fig. 12 Actual and tracked trajectories of the bead in the right path, as shown in the images of Fig. 9.

Conclusions

In this study, real-time imaging was used to track tracer particles with an integrated system that records, processes, and analyzes image data using advanced image-processing methods. Moreover, the system's ability to capture precise images and analyze them in real time demonstrates its potential for multiphase flow metering, making it an important area for future research.

The computational trajectory equation for the solid tracer particles, obtained using the CSRT tracking algorithm, showed a maximum error of ±5% relative to the actual trajectory equation, validating the accuracy of the proposed measurement system. This error, which essentially represents the percentage of trajectory conformity, results from a combination of experimental data acquisition, human error in extracting the actual trajectory equation, and the contour-locking mechanism applied by the tracking algorithm to the tracer particles in radiographic images.

With confidence in the proposed system, further research can focus on its ability to distinguish and track solid tracer particles of different sizes, materials, and densities. Moreover, extending the tracking process to other multiphase flows with a dispersed phase denser than the carrier fluid (such as sprays in fuel injection or solid particles suspended in liquid or gas beds), or with a carrier fluid denser than the dispersed phase (such as bubbles in gas injection into vertical liquid columns or liquid–solid mixtures), constitutes another direction for future studies. In these cases, and with reliance on the proposed system, the tracking of tracer particles within multiphase flows under different regimes, whether turbulent or laminar, can be investigated.

References

1. Zubakin, A. A., Davydov, A. I., Gogolev, A. S., Chistyakov, S. G., Filatov, N. A., Boyev, A. S., & Rukavishnikov, V. S. (2021, October). Development of an Innovational Multiphase X-Ray Flowmeter. In SPE Russian Petroleum Technology Conference (p. D031S014R005). SPE. https://doi.org/10.2118/206472-MS.
2. Kastengren, A., & Powell, C. F. (2007). Spray density measurements using X-ray radiography. Proceedings of the Institution of Mechanical Engineers, Part D: Journal of Automobile Engineering, 221(6), 653-662.
3. Lasheras, J. C., VILLERMAUX, E., & Hopfinger, E. J. (1998). Break-up and atomization of a round water jet by a high-speed annular air jet. Journal of Fluid Mechanics, 357, 351-379. doi.org/10.1017/S0022112097008070 .
4. Marmottant, P., & Villermaux, E. (2004). On spray formation. Journal of fluid mechanics, 498, 73-111. doi.org/10.1017/S0022112003006529 .
5. Varga, C. M., Lasheras, J. C., & Hopfinger, E. J. (2003). Initial breakup of a small-diameter liquid jet by a high-speed gas stream. Journal of Fluid Mechanics, 497, 405-434. doi.org/10.1017/S0022112003006724 .
6. Schumaker, S. A., Kastengren, A., Lightfoot, M. D., & Danczyk, S. (2012). A study of gas-centered swirl coaxial injectors using X-ray radiography (No. AFRLRZEDTP2012070).
7. Ma, J., van Ommen, J. R., Liu, D., Mudde, R. F., Chen,

X., Wagner, E. C., & Liang, C. (2019). Fluidization dynamics of cohesive Geldart B particles. Part I: X-ray tomography analysis. Chemical Engineering Journal, 359, 1024-1034. doi: 10.1016/j.cej.2018.11.082.

8. Escudero, D. R., & Heindel, T. J. (2014). Acoustic fluidized bed hydrodynamics characterization using X-ray computed tomography. Chemical Engineering Journal, 243, 411-420. Doi: 10.1016/j.cej.2014.01.025.
9. Alanazi, A.K., Alizadeh, S.M., Nurgalieva, K.S., Grimaldo Guerrero, J.W., Abo-Dief, H.M., Eftekhari-Zadeh, E., Nazemi, E. and Narozhnyy, I.M., 2021. Optimization of x-ray tube voltage to improve the precision of two phase flow meters used in petroleum industry. Sustainability, 13(24), p.13622. doi. org/10.3390/su132413622.
10. Aliseda, A., & Heindel, T. J. (2021). X-ray flow visualization in multiphase flows. Annual Review of Fluid Mechanics, 53(1), 543-567. doi.org/10.1146/annurev-fluid-010719-060201.
11. Salgado, C. M., de Freitas Dam, R. S., de Carvalho Conti, C., & Salgado, W. L. (2021). Three-phase flow meters based on X-rays and artificial neural network to measure the flow compositions. Flow Measurement and Instrumentation, 82, 102075. doi.org/10.1016/j.flowmeasinst.2021.102075.
12. Fiore, M., Razali, M. A. B., Zhang, T., Yang, K., Jolivet, G., Husoschi, L., & Hussenet, J. P. (2024, February). Improving Multiphase Flowmeter Accuracy for Hydrocarbon Allocation and Wet Gas Production of Unconventional Oil-Gas Wells. In International Petroleum Technology Conference (p. D011S029R009). IPTC. doi.org/10.2523/IPTC-23942-MS.
13. Misawa, M., Tiseanu, I., Prasser, H. M., Ichikawa, N., & Akai, M. (2022). Ultra-fast x-ray tomography for multi-phase flow interface dynamic studies. Kerntechnik, 68(3), 85-90.
14. Ge, M., Sun, C., Zhang, X., Coutier-Delgosha, O., & Zhang, G. (2022). Synchrotron X-ray based particle image velocimetry to measure multiphase streamflow and densitometry. Radiation Physics and Chemistry, 200, 110395. doi.org/10.1016/j.radphyschem.2022.110395.
15. Roshani, G.H., Muhammad Ali, P.J., Mohammed, S., Hanus, R., Abdulkareem, L., Alanezi, A.A., Nazemi, E., Eftekhari-Zadeh, E. and Kalmoun, E.M., 2021. Feasibility study of using X-ray tube and GMDH for measuring volume fractions of annular and stratified regimes in three-phase flows. Symmetry, 13(4), p.613.
16. Lukezic, A., Vojir, T., ˇCehovin Zajc, L., Matas, J., & Kristan, M. (2017). Discriminative correlation filter with channel and spatial reliability. In Proceedings of the IEEE conference on computer vision and pattern recognition (pp. 6309-6318).